Hybrid surface roughening modes during low-temperature heteroepitaxy: Growth of fully-strained metastable $Ge_{1-x}Sn_x$ alloys on Ge(001)2×1

P. Desjardins, T. Spila, O. Gürdal,* N. Taylor, and J. E. Greene
Materials Science Department, Coordinated Science Laboratory, and Materials Research Laboratory, University of Illinois, 1101 West Springfield Avenue, Urbana, Illinois 61801

(Received 15 July 1999)

Fully-strained single-crystal metastable $Ge_{1-x}Sn_x$ alloys were grown on Ge(001) up to their critical epitaxial thickness values $t_{epi}(x)$ in order to probe surface roughening pathways leading to heteroepitaxial breakdown during low-temperature molecular-beam epitaxy under large compressive strain. All films with $x>0.09$ have comparable roughnesses while films with $x<0.09$ are considerably rougher with larger lateral feature sizes. Roughening rates increase with increasing x for films with $x>0.09$ due to a new hybrid relaxation path which only becomes accessible under high strain as kinetic roughening provides surface oscillations on lateral length scales that allow bulk relaxation through strain-induced islanding at growth temperatures where it could not otherwise proceed. [S0163-1829(99)01247-3]

I. INTRODUCTION

The development of a detailed atomic-level understanding of surface morphological evolution during epitaxial growth is of intense current interest for both scientific and technological reasons. The two primary roughening mechanisms, kinetic roughening and strain-induced roughening, are typically associated with low-temperature (LT) homoepitaxy and high-temperature strained-layer heteroepitaxy, respectively. Our results show that this description is incomplete; the two mechanisms can interact to provide hybrid surface relaxation pathways during LT molecular-beam epitaxy (MBE) of highly-strained heteroepitaxial layers.

Kinetic roughening during low-temperature epitaxial growth[1–4] has been shown to be due to Ehrlich barriers to the migration of adatoms over down-steps and/or deep traps at up steps on growing surfaces.[5] This leads to a divergence in adatom flux and, hence, increased nucleation on terraces, which, in turn, gives rise to surface roughening and faceting with increasing film thickness. At some point, the growth front breaks down, presumably near the bottom of interisland trenches on rough surfaces,[6] in an irreversible transition to amorphous layer growth. For LT Si(001) (Refs. 6 and 7) and Ge(001) (Ref. 8) homoepitaxy, the surface roughness increases linearly with film thickness while the transition thickness decreases approximately exponentially with decreasing growth temperature T_s. Recent results from LT ($T_s=100-250\,^\circ C$) heteroepitaxy studies of strained $Si_{0.7}Ge_{0.3}$ alloys on Si(001) showed that kinetic roughening was also the dominant mechanism controlling surface morphological evolution.[3,9] The alloy surfaces exhibited small compact islands similar to LT Si(001) homoepitaxy but were found to be considerably smoother at the same growth temperature[9] due to a larger surface adatom mobility and/or a smaller edge barrier.[3]

In contrast, strain-induced roughening occurs during elevated-temperature heteroepitaxy of compressively strained layers to provide partial relaxation of the film strain energy through lateral expansion (compression) of the vertical planes in the surface mounds (valleys).[10–11] Equilibrium total-energy considerations indicate that strain-induced roughening is favorable at large lattice constant mismatch where the energy gain due to elastic relaxation is larger than the energy cost due to increased surface area.[11] Thus, there is a critical surface perturbation wavelength for a given materials system.[3,11–12] Development of the relatively large perturbation wavelengths associated with strain-induced roughening, typically $\simeq$1000–4000 Å,[10–11] usually requires elevated growth temperatures due to the necessity for significant mass transport.

The present experiments were undertaken in order to provide a more detailed understanding of surface roughening pathways leading to epitaxial breakdown[6,8,13] during LT-MBE of layers under large compressive strain. We chose $Ge_{1-x}Sn_x$/Ge(001) as a model system due to the 14.7% lattice constant mismatch between α-Sn ($a_{\alpha\text{-Sn}}=6.4892$ Å) and Ge ($a_{Ge}=5.6579$ Å). $Ge_{1-x}Sn_x$ and related alloys are themselves of interest due to the potential they offer for developing totally group-IV-based optoelectronic materials systems. $Ge_{1-x}Sn_x$ is predicted to exhibit a direct band gap in unstrained alloys, tunable from $\simeq$0.55 to 0 eV with x ranging from 0.20 to 0.65.[14–17] The growth of these alloys, however, presents severe challenges. The equilibrium solid solubility of Sn in Ge is less than 1 at % (Ref. 18) and Sn has a very strong tendency to surface segregate.[19–20]

We have recently demonstrated LT-MBE of fully-strained $Ge_{1-x}Sn_x$ alloys[21,22] and Ge/$Ge_{1-x}Sn_x$ superlattices[23] with x up to 0.26. Film growth temperatures T_s were confined to a very narrow range around $T_s=100\,^\circ C$ by the combination of increased kinetic roughening at lower growth temperatures and Sn surface segregation at higher temperature. Growth at such low temperature introduces, as noted above, a limit to the thickness of epitaxial material that can be grown prior to epitaxial breakdown. Figure 1 (see Ref. 21 for details) is a plot of $Ge_{1-x}Sn_x$ critical epitaxial thicknesses t_{epi} vs x. We define t_{epi} as the alloy layer thickness at which the amorphous phase is first observed in cross-section transmission electron microscopy (XTEM).

 ©1999 The American Physical Society

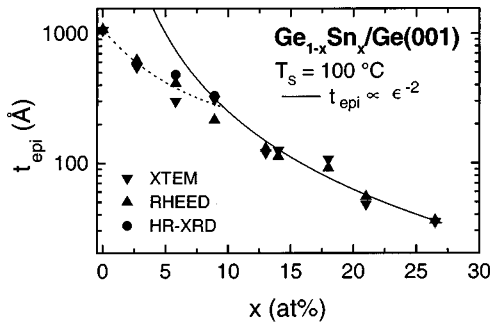

FIG. 1. Epitaxial thickness t_{epi} as a function of the Sn fraction x in $Ge_{1-x}Sn_x$ layers grown on Ge(001) at $T_s = 100\,°C$ (From Ref. 21). The solid line is calculated for constant strain energy.

t_{epi} values in Fig. 1 agree well with layer thicknesses at which twin reflections are first observed in reflection high-energy electron diffraction (RHEED) patterns obtained during film growth and with results from post-deposition high-resolution x-ray diffraction (HR-XRD) curves from which we calculate, using the angular spacing between finite-thickness interference-fringes, the thickness of the *epitaxial* portion of the $Ge_{1-x}Sn_x$ films. Critical epitaxial thickness values decrease continuously with increasing Sn concentration, from $\simeq 1080$ Å for pure Ge to 330 Å for $Ge_{0.91}Sn_{0.09}$ to 35 Å for $Ge_{0.74}Sn_{0.26}$. There is, however, a change in $t_{epi}(x)$ curvature near $x = 0.09$ which we attribute, as discussed below, to a cross over from kinetic to strain-induced roughening.

In this paper, we present results on the surface morphological evolution of fully strained metastable epitaxial $Ge_{1-x}Sn_x$ alloys as a function of x. Quantitative analyses of atomic force microscopy (AFM) results from a series of alloys grown to thicknesses $t = t_{epi}(x)$ reveal that all films with $x > 0.09$ have comparable roughnesses while films with $x < 0.09$ are considerably rougher with larger lateral feature sizes and exhibit morphologies typical of kinetic roughening. The change in $Ge_{1-x}Sn_x$ roughening mechanisms and kinetics for alloys, as well as the change in $t_{epi}(x)$ curvature, with $x > 0.09$ is due to the appearance of a hybrid relaxation mechanism. This pathway only becomes accessible during low-temperature growth under high strain as kinetic roughening provides surface oscillations on lateral length scales, which allow bulk film relaxation through strain-induced islanding at temperatures where it could not otherwise proceed. The new relaxation pathway increases the overall film roughening rate.

II. EXPERIMENTAL PROCEDURE

$Ge_{1-x}Sn_x$ alloys were grown in a multichamber MBE system with a base pressure of 5×10^{-11} Torr. A magnetically focused electron-beam source and a pyrolytic BN effusion cell were used to evaporate 99.9999% pure Ge and 99.999% pure Sn, respectively. The Sn effusion cell temperature was continuously monitored and maintained constant during film growth, using proportional-band feedback control, to within ± 1 °C. Surface structural transitions were recorded by RHEED using a 20 keV primary electron beam which intercepted the sample at a grazing angle of $\simeq 2°$.

The substrates were polished $1.50 \times 2.25\,cm^2$ n-type Ge(001) wafers with room-temperature resistivities of $1-20\,\Omega$-cm ($n = 1 \times 10^{15} - 6 \times 10^{13}\,cm^{-3}$). Substrate cleaning consisted of ultrasonic degreasing, rinsing in deionized water to remove the native oxide, oxidation by an UV-ozone process,[24] degassing in ultra-high vacuum at 250 °C for 20 min, and desorption of the oxide layer at $T_s \geqslant 430\,°C$. This procedure provides clean Ge surfaces with sharp 2×1 RHEED patterns and no impurities detectable by Auger or x-ray photoelectron spectroscopy.[24] 1000 Å-thick Ge buffer layers were then deposited at 400 °C and a growth rate $R_{Ge} = 0.6\,Å\,s^{-1}$. The resulting Ge(001) surfaces exhibit sharp 2×1 RHEED patterns with Kikuchi lines and are atomically smooth with average terrace widths of $\simeq 1300$ Å as demonstrated by scanning tunneling microscopy.[1] Alloy layers were deposited at $T_s = 100\,°C$ with R_{Ge} maintained at 0.6 $Å\,s^{-1}$ while the Sn deposition rate was set to obtain the desired composition. Film growth temperatures were controlled to within ± 1 °C and absolute values are accurate to within ± 10 °C. The chamber pressure during deposition was $\leqslant 1 \times 10^{-8}$ Torr.

$Ge_{1-x}Sn_x$ film compositions were determined by Rutherford backscattering spectrometry using a 2-MeV He^+ probe beam incident at 15° relative to the sample surface normal with the detector set at a 150° scattering angle. Backscattered spectra were analyzed using the RUMP simulation program.[25] A combination of XTEM, HR-XRD, and reciprocal lattice mapping showed that the films are epitaxial, with no evidence of phase separation, and fully strained. XTEM examinations were carried out using a Hitachi H9000 microscope operated at 300 kV. Specimens were prepared by gluing two samples film to film and then cutting a vertical section which was thinned by mechanical grinding to a thickness of $\simeq 25\,\mu m$. Final thinning to electron transparency was done by Ar^+ ion milling in a liquid-N_2-cooled stage in which the incident beam angle and energy were progressively reduced from 15 to 11° and 5 to 3.5 keV in order to minimize radiation damage artifacts and to obtain samples with relatively even thickness distributions.

$Ge_{1-x}Sn_x$ surface morphology was investigated as a function of film composition using contact-mode AFM. The measurements were carried out in air using a Digital Instrument Nanoscope II microscope with oxide-sharpened Si_3N_4 tips having radii of 5–40 nm. Height-difference $G(\rho) = \langle |hj - hi|2 \rangle$ *and height-height* $H(\rho) = \langle h_i h_j \rangle$ *correlation functions—where* h is the height at positions i and j separated by a distance ρ and the brackets correspond to averages over the measured surface—were calculated from the AFM images to quantify surface roughening. The correlation functions are related to the surface width $\langle w \rangle$ through the relationship $2\langle w \rangle^2 = G(\rho) - 2H(\rho)$. $[G(\rho \rightarrow \infty)]^{1/2}$ is directly proportional to $\langle w \rangle$ in these experiments since $H(\rho \rightarrow \infty) \rightarrow 0$, consistent with the above STM results showing that the high-temperature Ge buffer layers used as substrates for $Ge_{1-x}Sn_x$ growth were extremely flat.

III. RESULTS

The low-growth temperatures required to inhibit Sn segregation during $Ge_{1-x}Sn_x$ MBE lead to surface roughening and limited epitaxial thicknesses t_{epi}. RHEED and XTEM observations show that at constant film composition x,

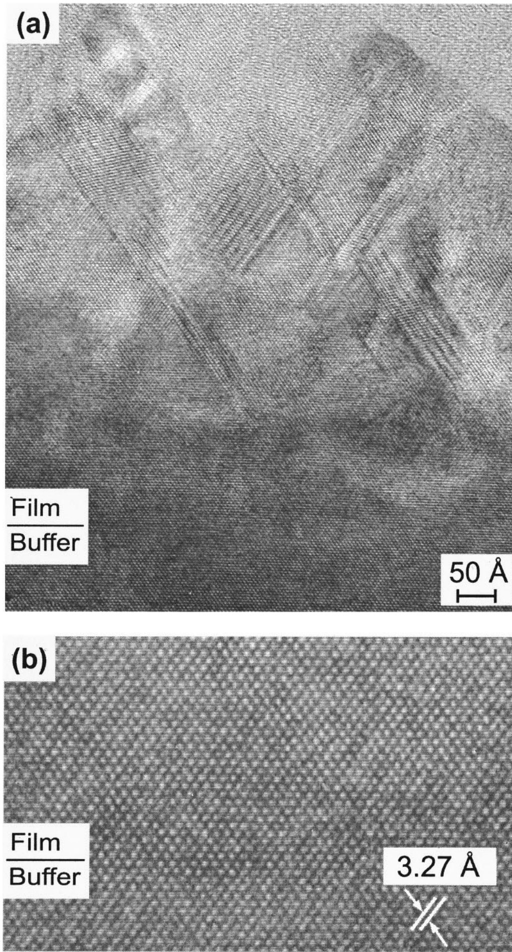

FIG. 2. (a) A high-resolution [110] XTEM micrograph from a $Ge_{0.91}Sn_{0.09}$ alloy grown on Ge(001) at $T_s = 100\,°C$ (b) A higher-resolution image of the structurally perfect region of the epitaxial sublayer.

roughening increases with film thickness t until epitaxial breakdown is observed. Moreover, comparing *in situ* RHEED results from films grown to the same thickness, surface roughness also increases with increasing Sn concentration. For all film compositions, RHEED patterns obtained during growth gradually transform with increasing film thickness from two dimensional to three dimensional with the appearance of $\frac{1}{3}$-order satellite reflections emanating from twinning on 111 planes.[21] With further deposition, bulk diffraction spot intensities decrease while diffuse scattering increases signaling an irreversible transition from epitaxial alloy growth to the terminal amorphous phase.

RHEED observations were confirmed by XTEM analyses showing three distinct sublayers in the films [Fig. 2(a)]. The alloys initially grow as highly structurally perfect single-crystal layers which are fully commensurate with the substrate. A higher magnification image of the first sublayer [Fig. 2(b)] reveals 111 lattice fringes which are continuous across the film/buffer-layer interface. The second sublayer is characterized by the formation of stacking faults and microtwins on 111 planes, consistent with RHEED results, together with increased surface roughening. Projections of the pyramidal islands are viewed as triangular-shaped objects in the XTEM image. The defective epitaxial layer terminates at a jagged, but locally atomically abrupt, crystalline/amorphous boundary. The terminal upper region is amorphous. We define t_{epi} as the point at which the amorphous phase is first observed. That is, t_{epi} is the minimum epitaxial thickness at breakdown. Values were obtained from examination of XTEM micrographs corresponding to more than 2 μm of interface for each sample composition.

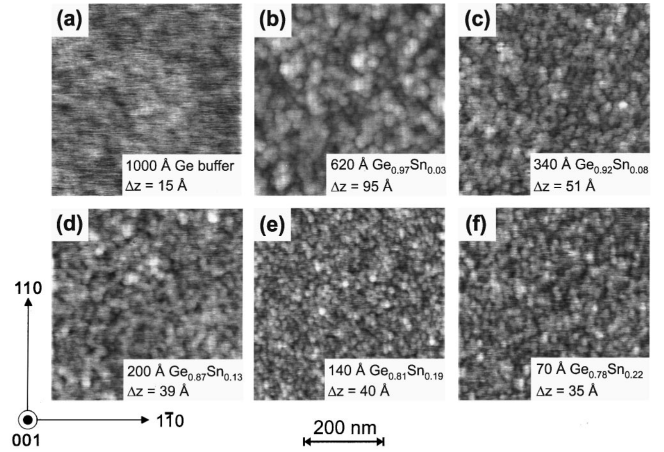

FIG. 3. AFM images of the surfaces of (a) a 1000 Å-thick Ge(001) buffer layer grown at $T_s = 400\,°C$ and (b)–(f) $Ge_{1-x}Sn_x(001)$ alloy layers grown at $T_s = 100\,°C$ to thicknesses $t = t_{epi}(x)$: (b) $x = 0.03$, $t = 620$ Å, (c) $x = 0.08$, $t = 340$ Å, (d) $x = 0.13$, $t = 200$ Å, (e) $x = 0.19$, $t = 140$ Å, and (f) $x = 0.22$, $t = 70$ Å. Δz is the black-to-white gray scale value.

As shown in Fig. 1, t_{epi} values for $Ge_{1-x}Sn_x$ on Ge(001) decrease continuously from 1080 Å for pure Ge to 330 Å for $Ge_{0.91}Sn_{0.09}$ to 35 Å for $Ge_{0.74}Sn_{0.26}$. In addition, and of more immediate interest in the present paper, we note that there is a change in $t_{epi}(x)$ curvature near $x \simeq 0.09$. This suggests that a new mechanism, in addition to kinetic roughening, becomes significant in determining surface morphological evolution for alloys with $x > 0.09$.

The elastic strain-energy E_{elas} per unit interfacial area in a strained film can be expressed as[26]

$$E_{elas} = \frac{2\mu(1+\nu)}{1-\nu}\varepsilon^2 t, \tag{1}$$

in which μ and ν are the film shear modulus and Poisson ratio and ε is the film/substrate misfit strain. Assuming that epitaxial breakdown is controlled by surface roughening and that there is a critical strain energy for breakdown, we obtain that $t_{epi} \propto \varepsilon^{-2}$ when neglecting small changes[27] in elastic constants as a function of x. The solid line in Fig. 1 shows that $t_{epi}(x)$ results for alloy layers with $x = 0.09-0.26$ ($\varepsilon = 1.3-3.8\%$) are well described by a constant strain-energy curve.

$Ge_{1-x}Sn_x$ layers with x ranging from 0.03 to 0.22 were grown to thickness $t = t_{epi}(x)$ in order to investigate strain effects on surface morphology at epitaxial breakdown. Figure 3 shows typical AFM images obtained from the Ge buffer layer as well as representative $Ge_{1-x}Sn_x$ alloy layers with $t = t_{epi}$. The images were linearly planarized to remove sample tilting effects during AFM measurements. Black-to-white gray scale values Δz were chosen to be four times the standard deviation of the height distribution around the average value and are therefore approximately proportional to

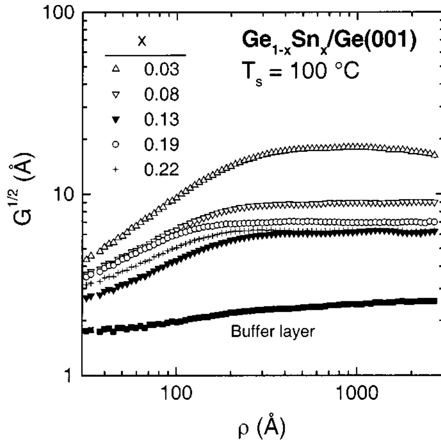

FIG. 4. Root-mean correlated height-difference $[G(\rho)]^{1/2}$ values vs the separation ρ of positions i and j on the surfaces of (a) a 1000 Å-thick Ge(001) buffer layer grown at $T_s=400\,°\mathrm{C}$ and (b)–(f) $\mathrm{Ge}_{1-x}\mathrm{Sn}_x(001)$ alloys grown at $T_s=100\,°\mathrm{C}$, (b) $x=0.03$, $t=620$ Å, (c) $x=0.08$, $t=340$ Å, (d) $x=0.13$, $t=200$ Å, (e) $x=0.19$, $t=140$ Å, and (f) $x=0.22$, $t=70$ Å.

$\langle w\rangle$. The surface of the 1000 Å-thick Ge buffer layer grown at $T_s=400\,°\mathrm{C}$ [Fig. 3(a)] is featureless and very flat with $\langle w\rangle=1.75$ Å.

All alloy surfaces appear qualitatively similar, exhibiting small compact rounded islands characteristic of kinetic roughening resulting from two-dimensional multilayer growth. We observe, however, significant differences in both lateral feature size $\langle d\rangle$ and surface width $\langle w\rangle$ as a function of alloy composition. All $\mathrm{Ge}_{1-x}\mathrm{Sn}_x$ layers with $x>0.09$ have comparable roughnesses while films with $x<0.09$ are significantly rougher and exhibit larger lateral feature sizes. These differences are quantified in Figs. 4 and 5. Figure 4 is a log-log plot of $[G(\rho)]^{1/2}$ vs ρ where $[G(\rho)]^{1/2}$ was obtained from 3000×3000 Å^2 images from four different regions of each sample while Fig. 5 is a plot of $\langle w\rangle$ and the average film roughening rate $\langle w\rangle/t$ vs x.

Figure 4 shows that in all cases, $[G(\rho)]^{1/2}$ initially increases with ρ following a power-law relationship. Effective roughening exponents α were determined from the data in Fig. 4 using the scaling relationship $G(\rho)\propto\rho^{2\alpha}$. Physically,

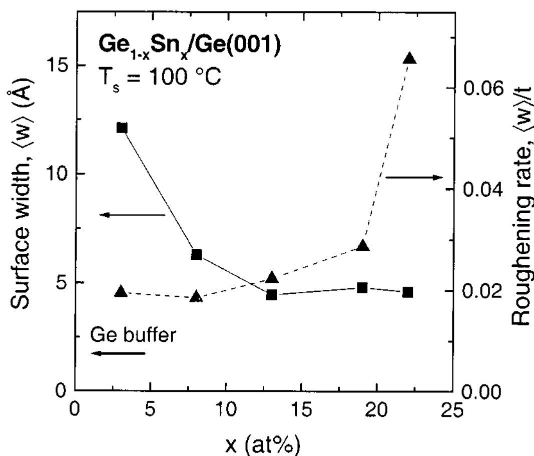

FIG. 5. Surface width $\langle w\rangle$ and average roughening rate ($\langle w\rangle/t$) vs the composition x of epitaxial $\mathrm{Ge}_{1-x}\mathrm{Sn}_x$ layers grown on Ge(001) to thicknesses $t=t_{\mathrm{epi}}$ at $T_s=100\,°\mathrm{C}$.

α is a measure of how well the roughness can be described by a single lateral length scale ($\alpha=1$). We find that α decreases continuously from 0.66 at $x=0.03$ to 0.45 for $x\geqslant0.13$. The smaller α values for alloys with larger Sn fractions indicate that the islands on these samples have less well-defined length scales. For comparison, α values for LT homoepitaxial growth of Si(001) (Ref. 3) and Ge(001) (Ref. 1) are 0.85 and 0.8, respectively.

$\langle w\rangle$ and the average lateral feature size $\langle d\rangle$ decrease from 12.1 and 300 ± 50 Å, respectively, for a 620 Å-thick $\mathrm{Ge}_{0.97}\mathrm{Sn}_{0.03}$ alloy to 6.3 and 225 ± 25 Å for a 340 Å-thick $\mathrm{Ge}_{0.92}\mathrm{Sn}_{0.08}$ alloy and then remain approximately constant at $\simeq4.6$ and 125 ± 25 Å, respectively, for alloys with $x=0.13$–0.22. $\langle d\rangle$ values obtained from the AFM images are consistent with XTEM observations of average island separations in samples of comparable composition deposited to $t>t_{\mathrm{epi}}(x)$.[21]

The average film roughening rate, $\langle w\rangle/t$, is constant at $\simeq$ 0.018 for alloys with $x\leqslant0.09$ (i.e., $\varepsilon\leqslant0.013$) and then increases continuously with x, to 0.066 for $x=0.22$. Based upon the results in Fig. 1, the elastic energy stored in all films with $x>0.09$ and grown to $t_{\mathrm{epi}}(x)$ is essentially the same, consistent with the notion that strain-induced roughening is playing an increasing role in the epitaxial breakdown process. However, the low-film growth temperature used in the present experiments, $T_s=100\,°\mathrm{C}$ would be expected to inhibit the large surface mass transport required for strain-induced roughening. The small $\langle d\rangle$ values, typical of kinetic roughening, are inherited from the initial stages of growth (see discussion below). For all $\mathrm{Ge}_{1-x}\mathrm{Sn}_x$ samples grown to $t=t_{\mathrm{epi}}$ irrespective of composition and strain, the aspect ratio $\langle w\rangle/\langle d\rangle$ is approximately constant at 0.030–0.050. This is evidence for a direct relationship between surface roughening and epitaxial breakdown.

IV. DISCUSSION

The results presented in the previous section show that the low-growth temperatures required to inhibit Sn segregation[21] during $\mathrm{Ge}_{1-x}\mathrm{Sn}_x$ LT-MBE lead to surface roughening and, ultimately, to epitaxial breakdown. Surface roughness increases with both film thickness and Sn fraction while t_{epi} values decrease rapidly with increasing x. $t_{\mathrm{epi}}(x)$ results for $x>0.09$ are well described by the relationship $t_{\mathrm{epi}}(x)\propto\varepsilon^{-2}$, where ε is the film/substrate misfit strain, indicating that there is a critical strain energy associated with epitaxial breakdown.

The reaction path leading to epitaxial breakdown was investigated using quantitative AFM analyses of films grown to $t=t_{\mathrm{epi}}(x)$. The surface morphology of all alloy layers is composed of small, 100–350 Å wide, compact rounded islands typical of kinetic roughening resulting from growth in the two-dimensional multilayer regime. In fact, all $\mathrm{Ge}_{1-x}\mathrm{Sn}_x$ AFM images in Fig. 3 are qualitatively similar to those characteristic of LT homoepitaxial Ge(001) (Refs. 1–2, 28) and Si(001).[3] Moreover the $\mathrm{Ge}_{1-x}\mathrm{Sn}_x(001)$ aspect ratio, $\langle w\rangle/\langle d\rangle$, at $t=t_{\mathrm{epi}}$ remains approximately constant, independent of ε (i.e., alloy composition).

Although the aspect ratio remains constant, the surface roughness of $\mathrm{Ge}_{1-x}\mathrm{Sn}_x$ layers with $t=t_{\mathrm{epi}}$ is significantly different in the low- and high-composition regimes as indi-

cated by the change in curvature of t_{epi} vs x. The surface morphologies of LT $Ge_{0.97}Sn_{0.03}$ and $Ge_{0.92}Sn_{0.08}$ layers are characteristic of kinetic roughening and quantitatively very similar to that of homoepitaxial Ge(001) layers of comparable thicknesses grown by MBE at the same substrate temperature.[1,2,28] As shown in Fig. 5, the average roughening rate is nearly constant at 0.018 for alloys with $x \leqslant 0.08$, suggesting that kinetic roughening remains the dominant mechanism controlling surface morphological evolution for these alloys layers.

In the higher alloy composition range ($x > 0.09$), the layers have much smaller mounds than in the dilute regime [compare, for example, Figs. 3(d)–3(f) with 3(b)–3(c)] and nearly identical surface roughness despite large changes in ε due to the increasing Sn fraction. However, the roughening rate increases by more than a factor of three as x is varied from 0.13 to 0.22. Thus, while these films exhibit features typical of kinetic roughening with in-plane correlation lengths of 100–150 Å (compared to 1000–4000 Å for strain-induced roughening), misfit strain clearly plays an ever increasing role in determining surface morphological evolution.

Relaxation through strain-induced roughening is thermodynamically favorable when the energy cost associated with the increased surface area is overcome by the gain (i.e., decrease) in film strain energy due to local lattice plane expansion/compression. Tersoff and LeGoues[29] showed that the activation energy for strain-induced roughening decreases rapidly with increasing misfit strain ε, varying as ε^{-4}. In contrast, the activation energy for dislocation nucleation and multiplication varies much more slowly with layer strain yielding a ε^{-1} dependence. Below a temperature-dependent critical film/substrate misfit, strain energy is relaxed by the nucleation of dislocations before the surface has time to roughen. Similarly, the temperature at which strain-induced roughening becomes kinetically favored over misfit-dislocation nucleation decreases with increasing misfit.[30]

The critical perturbation wavelength λ_c at which the strained layer becomes unstable to roughening can be estimated based upon a simple one-dimensional stability analysis leading to the relationship[31]

$$\lambda_c = \frac{\pi\gamma}{(1+v)E}. \tag{2}$$

γ in Eq. (2) is the surface energy and E is the strain energy per unit volume, E_{elas}/t [see Eq. (1)]. Thus,

$$\lambda_c = \frac{\pi\gamma(1-v)}{2\mu(1+v)^2\varepsilon^2}. \tag{3}$$

Assuming linear interpolation of the materials constants between Ge and α-Sn,[32,33] we find from Eq. (3) that λ_c decreases from 1100 Å at $x=0.08$ ($\varepsilon=0.012$) to 400 Å at $x=0.13$ ($\varepsilon=0.019$) to 140 Å at $x=0.22$ ($\varepsilon=0.032$). The latter value is approximately equal to the feature size observed in the AFM images obtained from the $x=0.22$ alloy layer. For the intermediate film compositions, $0.09 < x < 0.22$, where the same lateral feature sizes are observed, thermodynamic arguments alone cannot explain the surface morphological evolution. We propose, as discussed below, that kinetic roughening in this high-strain regime catalyzes strain-induced roughening.

Jesson *et al.*[10] noted that strain-induced surface roughening during MBE of compressive films occurs as a consequence of spatial gradients in the surface chemical potential μ. They recognized that such gradients will result in an atomic drift velocity and, following Refs. 12 and 34, derived equations for the time evolution of the surface profile during growth. The overall behavior is controlled by two primary competing terms. The first, which tends to flatten the profile, depends upon the local curvature of the surface while the second term involves the local stress tangential to the surface and gives rise to a net flux of adatoms from valleys toward peak regions. We propose that in the present LT heteroepitaxy experiments, kinetic roughening itself provides gradients in the surface chemical potential which, due to the relatively small perturbation wavelength, 100–150 Å, can initiate strain-induced roughening even at these low growth temperatures.

The above ideas can be assembled to describe surface roughening leading to epitaxial breakdown as a function of alloy composition during low-temperature heteroepitaxy of single-crystal alloys under increasing compressive strain. Low-temperature growth, even in the absence of strain (i.e., homoepitaxy), leads to the formation of small growth mounds for which the lateral length scales depend on adatom mobility, film growth rate, and island nucleation rates in a complex manner.

At small ε values (i.e., small gradients in chemical potential), strain-induced roughening requires long-perturbation wavelengths [Eq. (3)] and is highly kinetically constrained. The energy gain due to elastic strain relaxation is small because of the large energy cost associated with increased surface area. With increasing film thickness, the surface continues to roughen kinetically until breakdown occurs at a critical aspect ratio. The roughening rates for dilute $Ge_{1-x}Sn_x$ alloys with $x < 0.09$ ($\varepsilon < 0.013$) are nearly identical. The relatively slow decrease in t_{epi} with increasing x in this regime is attributed to a slight diminution in island size allowing the critical aspect ratio to be reached more rapidly for a constant roughening rate.

$\langle w \rangle$ and $\langle d \rangle$ remain constant for all films with $x > 0.09$ and $t = t_{epi}(x)$. Kinetic roughening in these layers during the initial stages of growth provides significant gradients in the surface chemical potential. This, in turn, leads to strain-induced roughening in which the lateral perturbation wavelength is determined by the initial gradients in chemical potential. The initial mound distribution acts as a template and the in-plane perturbation wavelength remains unchanged during subsequent growth to $t = t_{epi}$. Strain enhances the overall roughening rate[10] thus causing the critical aspect ratio for epitaxial breakdown to be reached at lower film thicknesses with increasing x since the lateral length scale is fixed by kinetically induced mound formation during the early stages of growth.

Finally, we point out that equilibrium critical perturbation wavelengths λ_c decrease rapidly with increasing ε. During heteroepitaxial growth at a given T_s, increasing x (or ε) corresponds to an increase in the film total energy. For very large ε values, the range of temperatures between kinetic

roughening and strain-induced roughening is dramatically reduced and can even overlap as shown by our results.

V. CONCLUSION

Fully strained single-crystal metastable $Ge_{1-x}Sn_x$ alloys were deposited on Ge(001)2×1 by solid-source molecular-beam epitaxy at 100 °C. $t_{epi}(x)$ values were found to decrease continuously from 1080 Å for pure Ge to 330 Å for $Ge_{0.91}Sn_{0.09}$ to 35 Å for $Ge_{0.74}Sn_{0.26}$. The surface morphology of films grown to thicknesses $t = t_{epi}(x)$ has been investigated by AFM. $\langle w \rangle$ and the average lateral feature size $\langle d \rangle$ decrease from 12.1 and 300±50 Å, respectively, for a 620 Å-thick $Ge_{0.97}Sn_{0.03}$ alloy to 6.3 and 225±25 Å for a 340 Å-thick $Ge_{0.92}Sn_{0.08}$ alloy and then remain approximately constant at ≃4.6 and 125±25 Å, respectively, for alloys with $x = 0.13-0.22$. The AFM results are consistent with the $t_{epi}(x)$ curve for which we note a change in curvature near $x = 0.09$. Surface morphologies of films with $x < 0.09$ consist of small, compact rounded islands, typical of kinetic roughening. $t_{epi}(x)$ results for $x > 0.09$ are well described by the relationship $t_{epi}(x) \propto \varepsilon^{-2}$ where ε is the misfit strain, suggesting that there is a critical strain energy for epitaxial breakdown. AFM results from all layers with $x > 0.09$ exhibit comparable $\langle w \rangle$ and $\langle d \rangle$ values corresponding to increased roughening rates with increasing x. We propose that the thermal activation required for the crossover from kinetic to strain-induced roughening is partially overcome by the fact that kinetic roughening provides local surface chemical potential gradients over lateral length scales, which are sufficiently small to initiate strain-induced roughening even at these low growth temperatures.

ACKNOWLEDGMENTS

This material is based upon work supported by the U.S. Department of Energy, Division of Materials Sciences under Grant No. DEFG02-ER9645439. P.D. was partially supported by the Natural Sciences and Engineering Research Council (NSERC) of Canada.

*Present address: Department of Electrical Engineering, Virginia Commonwealth University, Richmond, Virginia 23284-3072.

[1] J. E. Van Nostrand, S. J. Chey, M.-A. Hasan, D. G. Cahill, and J. E. Greene, Phys. Rev. Lett. **74**, 1127 (1995).
[2] J. E. Van Nostrand, S. J. Chey, and D. G. Cahill, Phys. Rev. B **57**, 12 536 (1998).
[3] N.-E. Lee, D. G. Cahill, and J. E. Greene, Phys. Rev. B **53**, 7876 (1996).
[4] B. W. Karr, I. Petrov, P. Desjardins, D. G. Cahill, and J. E. Greene, Surf. Coat. Technol. **94–95**, 403 (1997).
[5] S. C. Wang and G. Ehrlich, Phys. Rev. Lett. **70**, 41 (1993); **71**, 4177 (1993); G. Ehrlich, Surf. Sci. **331/333**, 865 (1995); A. Gölzhäuser and G. Ehrlich, Phys. Rev. Lett. **77**, 1334 (1996).
[6] D. J. Eaglesham, J. Appl. Phys. **77**, 3597 (1995).
[7] D. J. Eaglesham, H.-J. Gossman, and M. Cerullo, Phys. Rev. Lett. **65**, 1227 (1995).
[8] G. Xue, H. Z. Xiao, M.-A. Hasan, J. E. Greene, and H. Birnbaum, J. Appl. Phys. **74**, 2512 (1993).
[9] N.-E. Lee, D. G. Cahill, and J. E. Greene, J. Appl. Phys. **80**, 2199 (1996).
[10] D. E. Jesson, S. J. Pennycook, J.-M. Baribeau, and D. C. Houghton, Phys. Rev. Lett. **71**, 1744 (1993).
[11] A. G. Cullis, Mater. Res. Bull. **21**, 21 (1996).
[12] D. J. Srolovitz, Acta Metall. **37**, 621 (1989).
[13] N.-E. Lee, G. Xue, and J. E. Greene, J. Appl. Phys. **80**, 769 (1996).
[14] S. Groves and W. Paul, Phys. Rev. Lett. **11**, 194 (1963).
[15] S. Oguz, W. Paul, T. F. Deutsch, B.-Y. Tsaur, and D. V. Murphy, Appl. Phys. Lett. **43**, 848 (1983).
[16] D. W. Jenkins and J. D. Dow, Phys. Rev. B **36**, 7994 (1987).
[17] K. A. Mäder, A. Baldereschi, and H. von Känel, Solid State Commun. **89**, 1123 (1989).
[18] Bull. Alloy Phase Diagrams **5**, 266 (1984), and references therein.
[19] P. R. Pukite, A. Harwit, and S. S. Iyer, Appl. Phys. Lett. **54**, 2142 (1989).
[20] W. Wescheider, J. Olajos, U. Menczigar, W. Dondl, and G. Abstreiter, J. Cryst. Growth **123**, 75 (1992).
[21] O. Gurdal, P. Desjardins, J. R. A. Carlsson, N. Taylor, H. H. Radamson, J.-E. Sundgren, and J. E. Greene, J. Appl. Phys. **83**, 162 (1998).
[22] M. Roja-López, H. Navarro-Contreras, P. Desjardins, O. Gurdal, N. Taylor, J. R. A. Carlsson, and J. E. Greene, J. Appl. Phys. **84**, 2219 (1998).
[23] O. Gurdal, M.-A. Hasan, M. R. Sardela, Jr., J. E. Greene, H. H. Radamson, J.-E. Sundgren, and G. V. Hansson, Appl. Phys. Lett. **67**, 956 (1995).
[24] X.-J. Xhang, G. Xue, A. Agarwal, R. Tsu, M.-A. Hasan, J. E. Greene, and A. Rockett, J. Vac. Sci. Technol. A **11**, 2553 (1993).
[25] J. R. Doolittle, Nucl. Instrum. Methods Phys. Res. B **15**, 227 (1986).
[26] R. People and J. C. Bean, Appl. Phys. Lett. **47**, 322 (1985).
[27] This simple analysis ignores changes in the surface energy and elastic constants as a function of alloy composition. However, these changes are small, less than 13% over the entire range of x values investigated, while t_{epi} varies by more than a factor of 30, from 1080 Å for pure Ge to 35 Å for $Ge_{0.76}Sn_{0.24}$.
[28] J. E. Van Nostrand, Ph.D. thesis, University of Illinois at Urbana-Champaign, 1996.
[29] J. Tersoff and F. K. LeGoues, Phys. Rev. Lett. **72**, 3570 (1994).
[30] N.-E. Lee, M. Matsuoka, M. R. Sardela, Jr., F. Tian, and J. E. Greene, J. Appl. Phys. **80**, 812 (1996).
[31] H. Gao, J. Mech. Phys. Solids **42**, 741 (1994).
[32] K.-N. Tu, J. W. Mayer, and L. C. Feldman, *Electronic Thin Film Science for Electrical Engineers and Materials Scientists* (MacMillan, New York, 1992).
[33] *Semiconductors—Basic Data*, edited by O. Madelung, 2nd ed. (Springer-Verlag, Berlin, 1996).
[34] W. W. Mullins, J. Appl. Phys. **28**, 333 (1957).